Supporting Information

Ion Transport in Electrically Imperfect Nanopores

Yechan Noh and Narayana R. Aluru*

Department of Mechanical Science and Engineering, Beckman Institute for Advanced Science and Technology, University of Illinois at Urbana-Champaign, Champaign, Illinois 61820, United States

* *Corresponding Author / E-mail:* aluru@illinois.edu

Ionic conductance modeling

The analogy between electron transport in a conductive wire and ion transport through a channel suggests that ion conductance is proportional to the channel cross-section area divided by the channel length. However, this is not the case for short channels ($L \lesssim D$) where the access resistance plays a considerable role in the total resistance.

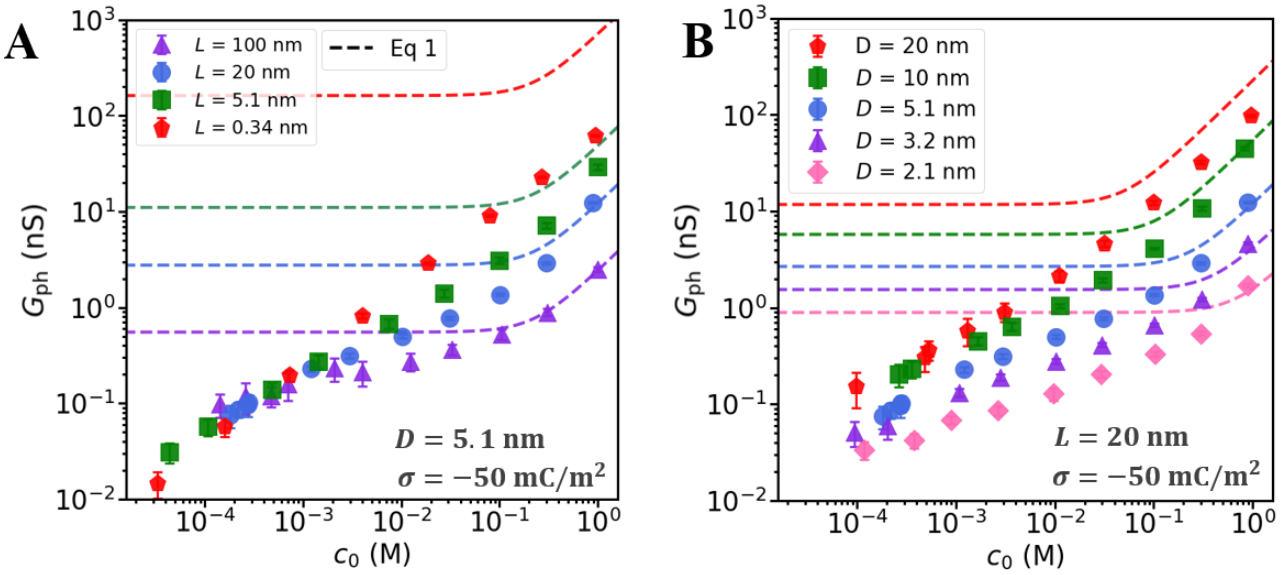

Figure S1. Ion conductance *versus* reservoir concentration for various (A) lengths and (B) diameters. The dashed lines are the conductance model without access resistance (Eq 1 of the main manuscript). The symbols are MD simulation data obtained using implicit water.

Figure S1 shows that the conductance model without the access resistance (Eq 1 of the main manuscript) overestimates the conductance even at high concentration. As discussed in the main text, the conductance model with access resistance (Eq 4 of the main manuscript) can accurately describe the conductance at high concentration (bulk transport dominant regime).

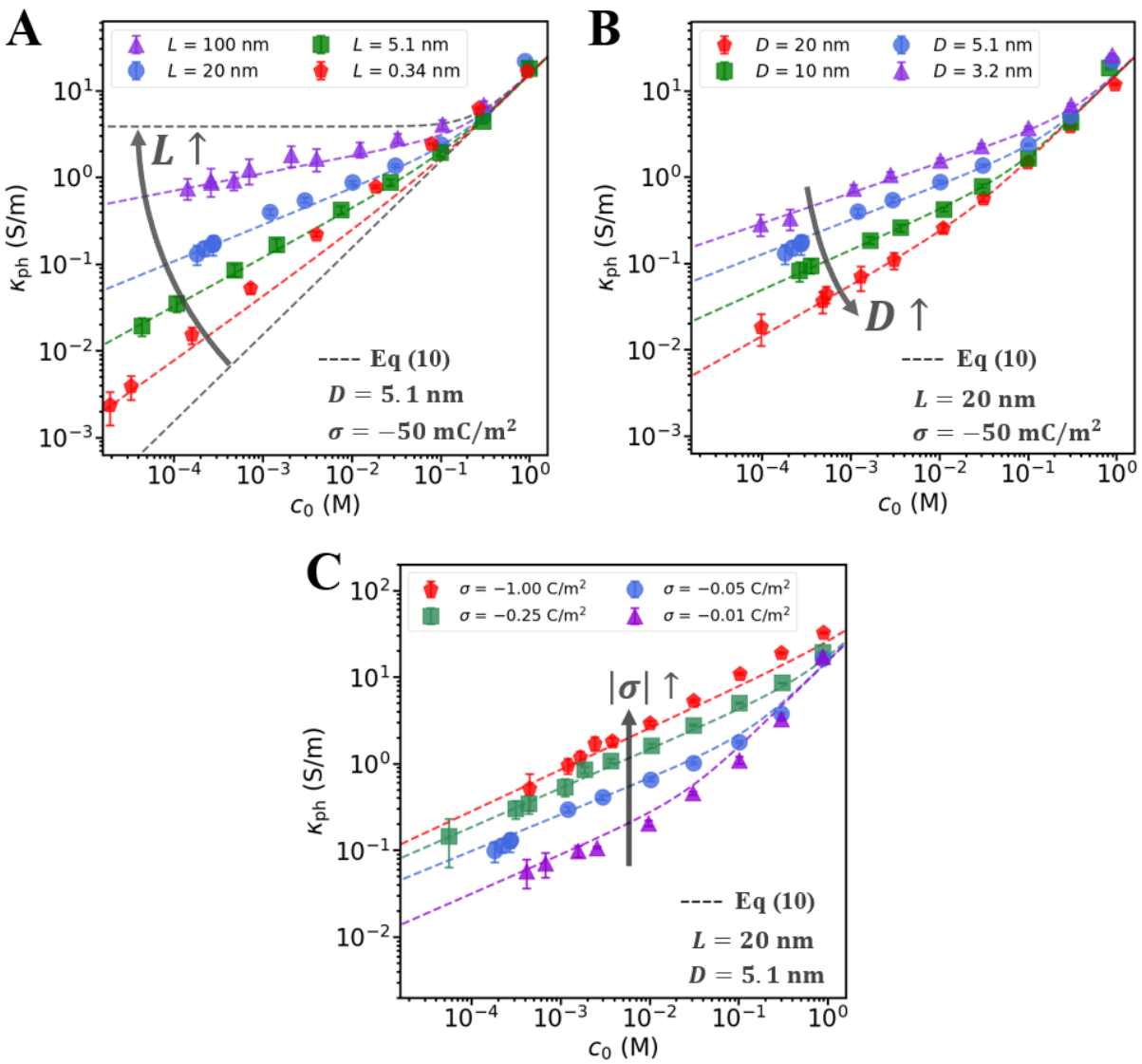

Figure S2. Ionic conductivity *versus* reservoir ion concentration for various (A) lengths (B) diameters (C) surface charge densities. The dashed lines are Eq 10 (see main manuscript) and α is obtained from fit to the data. The dashed gray lines in subplot (A) represent the bulk transport with $\alpha = 1$ (bottom line) and the conductance saturation with $\alpha = 0$ (top line).

Figure S2 shows that the conductivity model (Eq 10, main manuscript) describes the MD simulation data quite well. The ion conductivity can be regarded as the conductance normalized by the geometrical parameters, *i.e.*, $\kappa = G\left(\frac{L}{\pi R^2} + \frac{1}{2R}\right)$. As a result, the bulk conductivity, $Fc_0(\mu_+ + \mu_-)$, is independent of the channel geometry. Hence, the conductivity of various channels overlaps at high concentrations. At low concentration, however, the conductivity depends on the channel geometry as the electric-potential-leakage (power-laws) is related to the aspect ratio of the channel.

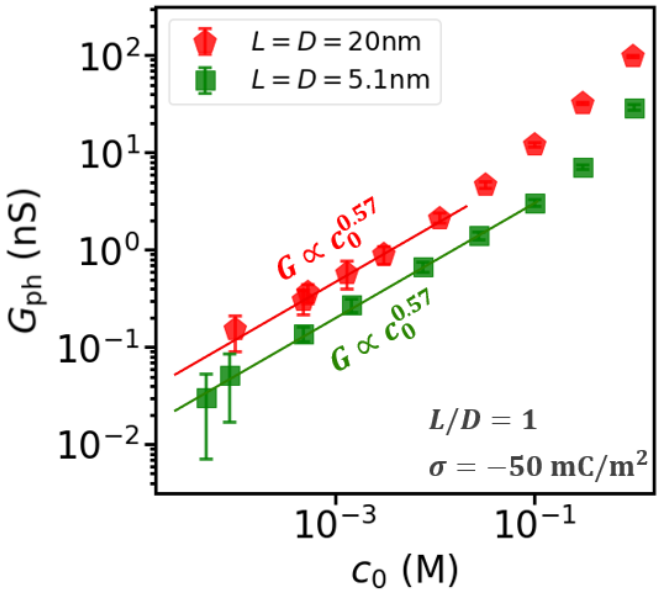

Figure S3. Ion conductance *versus* reservoir ion concentration for two different pores with an identical aspect ratio.

As discussed in the main manuscript, diameter and length have opposite effect on the power-law relation. Figure S3 shows that two different channels with an identical aspect ratio have very similar power-laws. Note that the larger channel (red) has approximately 16 times larger cross-section area than the smaller channel (green). This observation allows us to analyze the power law as a function of R/L.

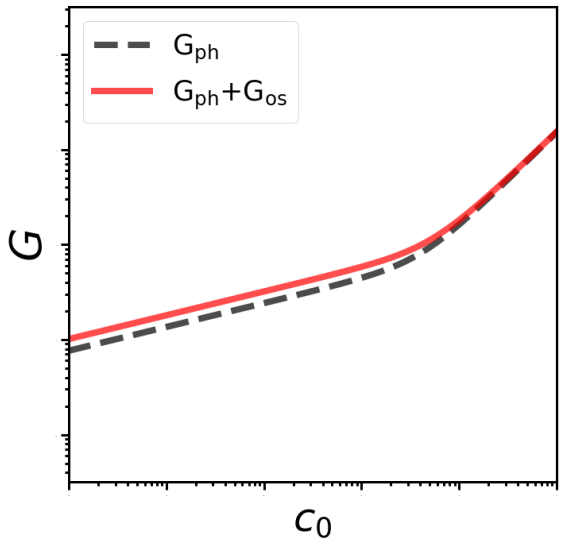

Figure S4. Conductance *versus* concentration curves in log-log scale with and without electroosmotic flow when the electroosmotic mobility is a constant.

Figure S4 shows that electroosmosis enhances the surface conductance while it does not enhance the bulk conductance as the bulk solution is electrically neutral (zero net charge). Also, the same power-law is predicted if electroosmotic mobility is assumed constant and independent of ion concentration.

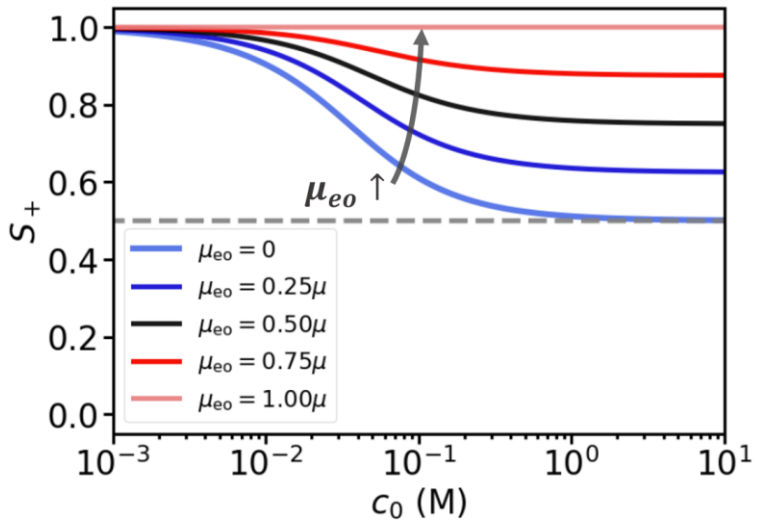

Figure S5. Effects of electroosmosis on ion-selectivity for various ion concentration ranges. The solid lines are Eq 16-17 of the main manuscript for cases with $\sigma = -0.01\ \mathrm{C/m^2}$, $\alpha = 0.5$ and $\mu = \mu_+ = \mu_-$. The electroosmotic mobility is assumed to be constant with respect to the ion concentration. Dashed line represents no selectivity with $S_+ = 0.5$ (bulk transport).

Figure S5 shows that ion selectivity increases as electroosmotic mobility increases and reaches the perfect selectivity limit when μ_{eo} is equal to the electrophoretic mobility. This suggests that enhancing the electroosmosis can improve the performance of nanopore-based electricity generation using sea water.

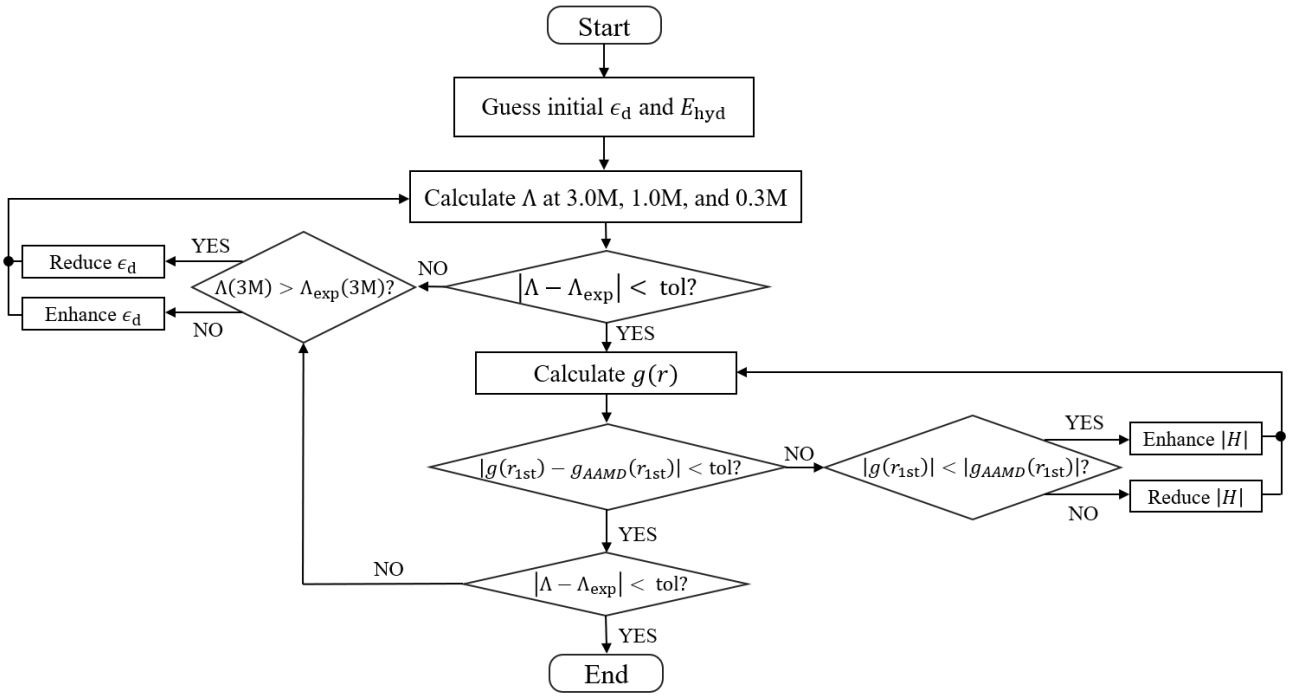

Figure S6. Schematic diagram of the optimization process of dielectric permittivity and hydration energy for an accurate prediction of RDFs, g(r), and concentration-dependent molar conductivity.

Development of implicit water forcefields for ion transport

The molar conductivity (Λ), defined as the ionic conductivity normalized by ion concentration, decreases as the concentration increases due to the increasing electrolyte friction.[1] This effect originates from the long-range interactions between ions and the combined atomic dynamics of solution. In aqueous solution, the inhomogeneous orientation of water molecules near ions creates an offset electric field that weakens the resulting Coulomb force. In the classical theory, this effect is considered as a constant dielectric permittivity ϵ_{d}. At the molecular scale, however, this screening effect depends on the distance between charges, $\epsilon_{\mathrm{d}}(r)$.[2–4] This distance-dependent dielectric function is closely related to the Radial Distribution Functions (RDFs) between ionic pairs and the concentration-dependent molar conductivity $\Lambda(\mathrm{c}_0)$. The hydration shells are formed near ions due to the strong non-bonded interaction between ions and water, E_{hyd}. This hydration energy affects the solution structure that is directly related to $\epsilon_{\mathrm{d}}(r)$. Therefore, the optimization of $\epsilon_{\mathrm{d}}(r)$ and E_{hyd} was done in a coupled manner. Figure S6 shows how these functions are optimized for an accurate prediction of $g(r)$ and $\Lambda(\mathrm{c}_0)$. The finalized $\Lambda(\mathrm{c}_0)$ and $g(r)$ obtained from the optimized $\epsilon_{\mathrm{d}}(r)$ and E_{hyd} are shown in Figure S7-8. The optimized parameters are listed in Table S1.

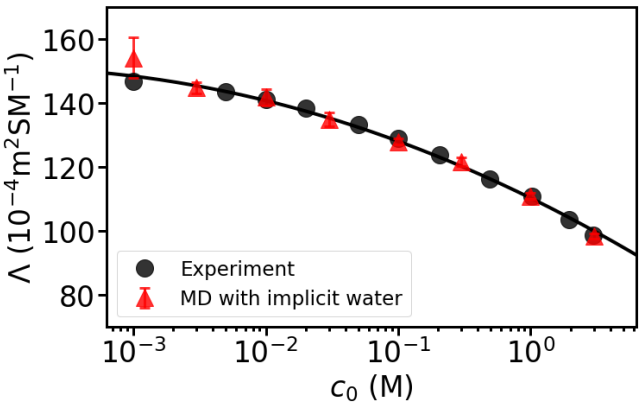

Figure S7. Concentration-dependent molar conductivity in aqueous KCl. The experimental data are from the CRC handbook[5].

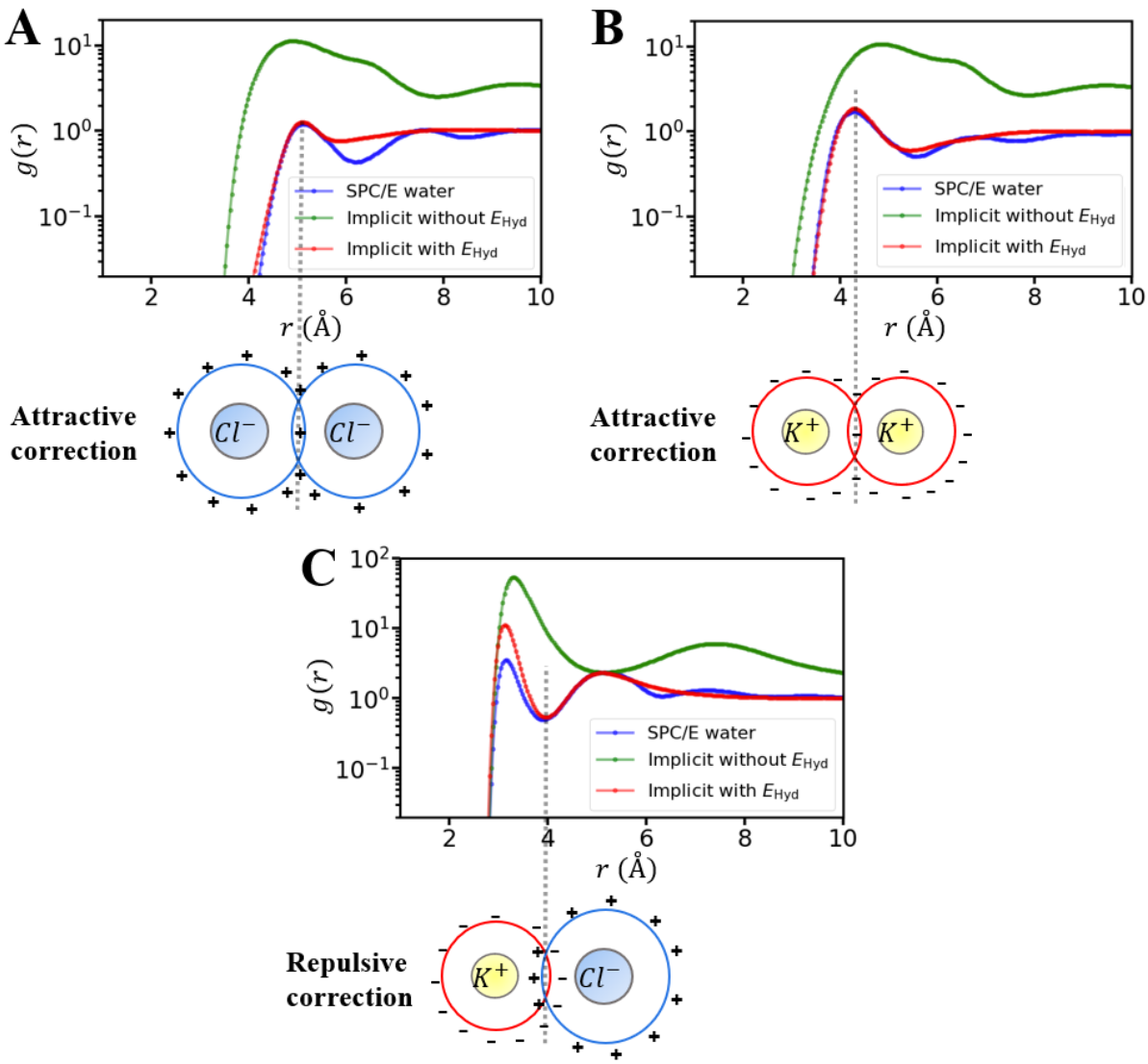

Figure S8. RDFs of all ionic pairs. (A) RDF between Cl^- ions, (B) RDF between K^+ ions, and (C) RDF between K^+ and Cl^-. The illustrations below each plot represent the first ionic hydration shell.

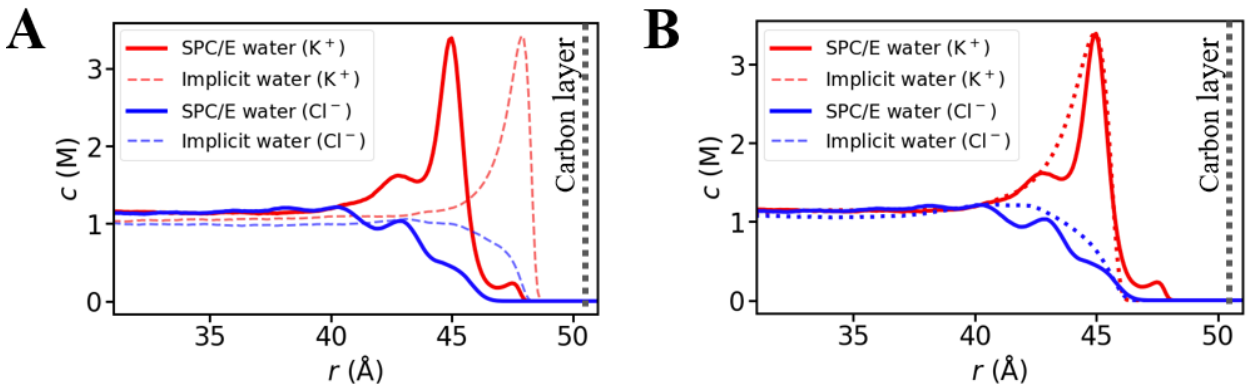

Figure S9. EDL near a single layer of graphene (A) without wall hydration correction and (B) with wall hydration correction.

Hydration effects near the channel surface affect the Electrical Double Layer (EDL). By considering this effect, the wall-ion LJ potential is corrected to better reproduce the EDL. Figure S9 shows how the wall hydration correction on the implicit water forcefield effects the interfacial ionic structure.

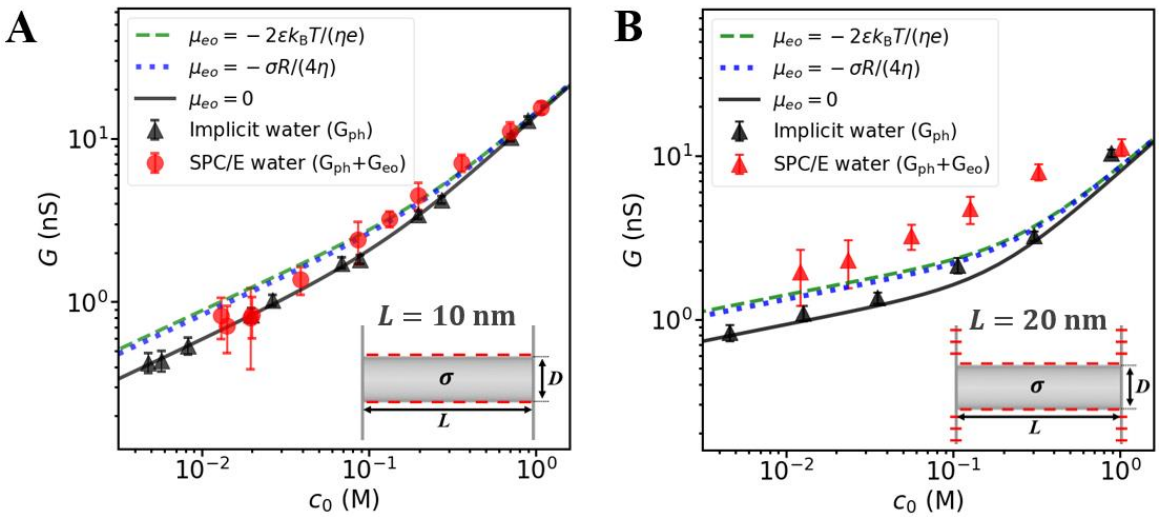

Figure S10. The benchmark studies of ion transport using coarse-grained MD with implicit water and all-atom MD with SPC/E water. (A) the channel is charged. (B) both the channel and the membrane are charged. $D = 5.1$ nm and $\sigma = -50$ mC/m^2 for all cases. The lines are from Eq 13 (see the main manuscript).

Figure S10 shows the ionic conductance obtained from all-atom MD and MD with the implicit water force-field. MD with implicit water model only considers the electrophoretic transport. The theoretical model for electrophoretic conductance (Eq 11 of the main manuscript) describes quite well the MD data with implicit water. In the case of all-atom MD, electroosmosis enhances the surface conductance. The conductance model with electroosmosis (Eq 13 of the main manuscript) better predicts the all-atom MD data than the model without electroosmosis (Eq 11) but not as accurately as one would like. The benchmark data from MD simulations with SPC/E and implicit water show that the power-law depends weakly on electroosmosis for the tested cases.

Table S1. Optimized potential parameters for implicit water and explicit ions.

Pair	Potential	Potential Parameters			Sources
		σ_{LJ} [Å]	ϵ_{LJ} [Kcal/mol]		
C - C	LJ	3.3900	0.0692		Werder *et al.*[6]
Cl^- - Cl^-		4.8305	0.0128		Joung *et al.*[7]
K^+ - K^+		2.8384	0.4297		
C - Cl^-		7.9800	0.0001		EDL optimization
C - K^+		5.9400	0.0120		
Cl^- - K^+		3.8345	0.0742		L-B Mixing Rule
	Gaussian	H [Kcal · Å/mol]	r_{mh} [Å]	σ_{h} [Å]	RDF and $\Lambda(c_0)$ optimization
Cl^- - Cl^-		-0.870	4.930	0.40	
K^+ - K^+		-4.020	3.900	0.65	
Cl^- - K^+		6.150	3.550	0.67	
	Dielectric permittivity	ϵ_s	r_{me} [Å]	σ_ϵ [Å]	RDF and $\Lambda(c_0)$ optimization
All pairs		78	4.917	1.88	

Table S2. Force-fields parameters for all-atom MD

	σ_{LJ} [Å]	ϵ_{LJ} [Kcal/mol]	Reference
C - C	3.3900	0.0692	Werder *et al.*[6]
O - O	3.1656	0.1554	SPC/E[8]
H - H	0.0000	0.0000	
Cl^- - Cl^-	4.8305	0.0128	Joung *et al.*[7]
K^+ - K^+	2.8384	0.4297	
C - O	3.4360	0.0850	Wu and Aluru[9]
C - H	2.6900	0.0383	
C - Cl^-	4.1103	0.0298	L-B Mixing Rule
C - K^+	3.1142	0.1724	
C - Cl^-	3.9981	0.0446	
O - K^+	3.0020	0.2584	
O - Cl^-	3.9981	0.0445	
H - ions	0.0000	0.0000	
Cl^- - K^+	3.8345	0.0742	
O - H	Hydrogen bonding		(SHAKE)

References

(1) Chandra, A.; Bagchi, B. Ion Conductance in Electrolyte Solutions. *J. Chem. Phys.* **1999**, *110*, 10024–10034.

(2) Teschke, O.; Ceotto, G.; de Souza, E. F. Interfacial Water Dielectric-Permittivity-Profile Measurements Using Atomic Force Microscopy. *Phys. Rev. E* **2001**, *64*, 011605.

(3) Fumagalli, L.; Esfandiar, A.; Fabregas, R.; Hu, S.; Ares, P.; Janardanan, A.; Yang, Q.; Radha, B.; Taniguchi, T.; Watanabe, K.; Gomila, G.; Novoselov, K. S.; Geim, A. K. Anomalously Low Dielectric Constant of Confined Water. *Science* **2018**, *360*, 1339–1342.

(4) Motevaselian, M. H.; Mashayak, S. Y.; Aluru, N. R. Extended Coarse-Grained Dipole Model for Polar Liquids: Application to Bulk and Confined Water. *Phys. Rev. E* **2018**, *98*, 052135.

(5) Haynes, W. M. *CRC Handbook of Chemistry and Physics*, 97th eds.; CRC Press: Boca Raton, FL, 2016; pp 940–943.

(6) Werder, T.; Walther, J. H.; Jaffe, R. L.; Halicioglu, T.; Koumoutsakos, P. On the Water−Carbon Interaction for Use in Molecular Dynamics Simulations of Graphite and Carbon Nanotubes. *J. Phys. Chem. B* **2003**, *107*, 1345–1352.

(7) Joung, I. S.; Cheatham, T. E. Determination of Alkali and Halide Monovalent Ion Parameters for Use in Explicitly Solvated Biomolecular Simulations. *J. Phys. Chem. B* **2008**.

(8) Berendsen, H. J. C.; Grigerra, J. R.; Strsstsma, T. P. The Missing Term in Effective Pair Potentials. *J. Phys. Chem.* **1987**, *91*, 6269–6271.

(9) Wu, Y.; Aluru, N. R. Graphitic Carbon–Water Nonbonded Interaction Parameters. *J. Phys. Chem. B* **2013**, *117*, 8802–8813.